Technical note: Identification of chemical composition and source of fluorescent components in atmospheric water-soluble brown carbon by excitation-emission matrix with parallel factor analysis: Potential limitation and application

Tao Cao[1,2,3], Meiju Li[1,2,3], Cuncun Xu[1,2,3], Jianzhong Song[1,2,5,*], Xinjun Fan[4], Jun Li[1,2,5], Wanglu Jia[1,2], Ping'an Peng[1,2,3,5]

[1]State Key Laboratory of Organic Geochemistry and Guangdong Provincial Key Laboratory of Environmental Protection and Resources Utilization, Guangzhou Institute of Geochemistry, Chinese Academy of Sciences, Guangzhou 510640, China

[2]CAS Center for Excellence in Deep Earth Science, Guangzhou 510640, China

[3]University of Chinese Academy of Sciences, Beijing 100049, China

[4]College of Resource and Environment, Anhui Science and Technology University, Fengyang 233100, China

[5]Guangdong-Hong Kong-Macao Joint Laboratory for Environmental Pollution and Control, Guangzhou 510640, China

[*]*Correspondence to:* Jianzhong Song, E-mail: songjzh@gig.ac.cn.

Abstract

Three-dimensional excitation-emission matrix (EEM) fluorescence spectroscopy is an important method for the identification of occurrences, chemical compositions, and sources of atmospheric chromophores. However, current knowledge on the identification and interpretation of fluorescent components is mainly based on aquatic dissolved organic matter and might not be applicable to atmospheric samples. Therefore, this study comprehensively investigated EEM data of different types of strong light-absorbing organic compounds, water-soluble organic matter (WSOM) in different aerosol samples (combustion source samples and ambient aerosols), soil dust, and purified fulvic and humic acids supplemented by parallel factor (PARAFAC) modelling. The results demonstrated that organic compounds with high aromaticity and strong electron-donating groups generally present strong fluorescence spectra at longer emission wavelengths, whereas organic compounds substituted with electron-withdrawing groups have relatively weaker fluorescence intensity. In particular, aromatic compounds containing nitro groups (i.e., nitrophenols), which show strong absorption and are the major component of atmospheric brown carbon, exhibited no significant fluorescence. EEM-PARAFAC identified three fluorescent components (i.e., C1, C2, and C3) in ambient WSOM. Although EEM-PARAFAC derived C1 (235, 270/330 nm) in ambient WSOM is generally considered as protein-like groups, our findings suggested that it is mainly composed of aromatic acids, phenolic compounds, and their derivatives, with only traces of amino acids. C2 is associated with the atmospheric chemical reaction of

biomass burning and/or biogenic organic molecules, with relatively lower degree of oxidation, which are more abundant in Guangzhou WSOM (56%-69%). Whereas, C3 is mainly attributed to highly oxygenated organic molecules derived from soil and atmospheric aging processes and has a relatively higher contribution in Chuzhou WSOM (23%). These findings provide new insights for the analysis of chemical properties and sources of atmospheric fluorophores using the EEM method.

1. Introduction

Water-soluble organic carbon (WSOC) constitutes a substantial fraction (10–80%) of organic aerosols in the atmosphere and is ubiquitous in ambient aerosols, clouds or fog, and rain water (Wozniak et al., 2012; Huang et al., 2022, Zhang et al., 2022a). Recent studies have highlighted that a portion of WSOC, termed brown carbon (BrC), can absorb light in the near-ultraviolet and visible ranges (Laskin et al., 2015, Frka et al., 2022; Ma et al., 2022). Owing to its strong light-absorption capacity, BrC can cause up to 45% solar radiation absorption by atmospheric aerosols and has potential effects on regional and even global climate (Zhang et al., 2013). In addition, BrC also participates in atmospheric photochemical reactions, affects the physicochemical properties of atmospheric aerosols (Laskin et al., 2015; Tang et al., 2020b), and potentially, can be activated to form reactive oxygen species that cause adverse effects on human health (Cao et al., 2021; Zhang et al., 2022b).

Excitation-emission matrix (EEM) fluorescence spectroscopy is a highly sensitive and widely used analytical technique for the identification of chemical

characteristics and sources of chromophores in dissolved organic matter (DOM) in aquatic environments (Murphy et al., 2010, 2013; Zhang et al., 2014). Recently, EEM has been further extended and frequently applied for the investigation of water-soluble organic matter (WSOM), such as light-absorbing organic compounds in atmospheric aerosols and fine particles from combustion processes (Chen et al., 2020; Fan et al., 2016; Wu et al., 2020; Yang et al., 2022). For instance, humic-like substances (HULIS) and protein-like substances (PRLIS) have been identified as important fluorescent components in combustion-derived particles (Cao et al., 2021; Tang et al., 2021) and ambient aerosols (Ma et al., 2022; Wu et al., 2020; Yang et al., 2022). Chen et al. (2016) used EEM coupled with parallel factor analysis (PARAFAC) and high-resolution mass spectrometry to identify chromophores in ambient aerosols and proposed that fluorescent components with longer excitation (Ex)/emission (Em) wavelengths comprise more highly oxygenated groups (Chen et al., 2016a). In addition, further application of the EEM method has also revealed that the concentration and types of fluorophores obviously vary during atmospheric processes, such as photolytic aging of biomass burning (BB)-derived chromophores (Aftab et al., 2018; Tang et al., 2020b). Therefore, the EEM method has significant potential for the characterization (types, sources, and evolution) of atmospheric BrC.

However, application of the EEM method for the identification of atmospheric BrC has some limitations. It is well known that the present identification, classification, and interpretation of fluorescent components in atmospheric WSOM are mainly based on the fluorescence peak position of DOM in aquatic environments

(Coble, 1996; Wünsch et al., 2019). Nonetheless, the chemical and molecular composition and source of WSOM in atmospheric aerosols significantly vary from those of DOM in aquatic environments (Graber and Rudich, 2006; Laskin et al., 2015); hence, the current fluorescence criterion derived from aquatic environments could lead to some inaccurate description of the fluorescent components in atmospheric WSOM. For instance, the EEM region at Ex/Em = 235(270)/330 nm is assigned to PRLIS and/or tryptophan-like substances in aquatic environments (Coble, 1996), but is also associated with non-nitrogen species such as polyphenols in atmospheric WSOM (Chen et al., 2016b). The EEM region at peak M (290–315/370–420 nm) is considered as a typical signal of marine-derived HULIS (Coble, 2007; Zhao et al., 2019), but the source of this peak should be cautiously investigated when interpreting BrC in continental aerosols. In addition, the intensities of fluorescent species are not always linearly correlated with their concentrations, which can be affected by the aromatic ring system and the number and types of functional groups, thereby leading to greater uncertainty in intensity measurements (Andrade-Eiroa et al., 2013; Chen et al., 2020; Wang et al., 2020). Atmospheric BrC is composed of complex organic molecules with different light absorption properties (Lin et al., 2020; Huang et al., 2021; Jiang et al., 2022), and only a subset of BrC molecules that contain functional groups are capable of fluorescence emission upon relaxation from an excited state (Andrade-Eiroa et al., 2013). Hence, interpretation of fluorescence data may only correspond to fluorescent chromophores and may not be representative of BrC as a whole (Chen et al., 2020;

Wang et al., 2020). All these factors limit further application of the EEM method for the analysis of atmospheric BrC. Therefore, it is essential to investigate the light-absorbing species that can be detected by EEM and obtain important information for identifying the chemical compositions and possible sources of these species.

Accordingly, in the present study, the EEM profiles of a series of BrC model compounds and WSOM isolated from primary combustion samples, soils, and atmospheric aerosols were investigated. The chemical characteristics and sources of the main fluorophores were interpreted according to the fluorescence peaks location and intensity, and the chemical structures of the model compounds and source samples were analyzed. Then, atmospheric aerosols in Guangzhou (GZ) and Chuzhou (CZ) cities were collected and fluorescent chromophores within the water-soluble fraction were identified to estimate the application of the EEM-PARAFAC method in characterizing atmospheric BrC. The results obtained help to broaden the application of the EEM-PARAFAC method to study atmospheric BrC.

2. Materials and methods

2.1. Materials

For accurate identification of the chemical composition and structures of fluorophores in atmospheric BrC and for assessment of application of the EEM method to examine atmospheric BrC, a total of 136 samples were investigated in this

study. The samples comprised: (1) 35 BrC model compounds, including phenolic compounds, aromatic acids, nitroaromatic compounds (NACs), PRLIS, N-heterocyclic compounds, and polycyclic aromatic hydrocarbons (PAHs) and their derivatives (detailed information in Text S1.1 and Table S1 of supporting information (SI)). These compounds are usually detected in ambient samples and have been considered typical BrC model compounds (Frka et al., 2022, Lin et al., 2016; 2017; Wang et al., 2017; Huang et al., 2021); (2) 13 primary combustion source samples collected from BB, coal combustion (CC), and vehicle emission (VE); (3) five soil samples obtained from the rural area of Guangdong Province, China, with different vegetation, which is also an important source of atmospheric BrC and has been widely identified in previous studies (Chen et al., 2020; Vasilatou et al., 2017); (4) six purified fulvic and humic acids (FAs and HAs, respectively) kindly provided by Professor Weilin Huang (Rutgers, The State University of New Jersey, NJ, USA); and (5) 34 diurnal fine particulate matter ($PM_{2.5}$) samples collected from 6 to 22 April, 2021 at GZ and CZ, respectively. In addition, 43 annual $PM_{2.5}$ samples were collected from February 2018 to January 2019 at the GZ site and classified as wet and dry season atmospheric $PM_{2.5}$ samples (for detailed information, see Text S1 of SI). Field blank samples were collected without instrument power on during each sampling period.

2.2. Standard solution and aqueous extraction of ambient samples

Solutions of model organic compounds were prepared by dissolving a certain

amount of dried solid or liquid samples in Milli-Q water or methanol. The ambient aerosol and soil samples were ultrasonically extracted with ultrapure water three times, and the supernatants were filtered using a 0.22-μm PTFE syringe filter to isolate the WSOM. The specific separation and purification methods have been published in previous studies (Chen et al., 2020; Fu et al., 2015; Wang et al., 2020; Yan and Kim, 2017) and are presented in the SI (Test S2).

2.3. EEM-PARAFAC analysis

The EEM fluorescence spectra of the aqueous extraction of the samples in 1-cm quartz cuvettes were recorded using a three-dimensional fluorescence spectrophotometer (Aqualog; HORIBA Scientific, USA) at room temperature. The scanning ranges for Ex and Em were 200–500 and 250–550 nm, respectively. The wavelength increment of the Ex and Em scans was 5 nm, the integration time was 0.5 s, and Milli-Q water (18.2 MΩ cm) used as blank reference. The absorbance measurements were used to correct the EEM for inner filter effects (IFEs) as described previously (Fu et al., 2015) if the absorbance was > 0.05 at 250 nm (Murphy et al., 2013; Tang et al., 2020a). Background samples were also analyzed and the background values were subtracted from the values obtained for all the samples. To avoid concentration effects, the fluorescence spectra were normalized by the water Raman area to produce Raman unit (R.U.) and further by the organic carbon concentration of the samples to the normalized fluorescence intensities (R.U./(mg C/L)) (Yang et al., 2022) are shown in Table S2.

The PARAFAC modelling procedure was conducted for 77 atmospheric WSOM samples in MATLAB 2014b (Mathwork.Inc, USA) using the drEEM toolkit (Murphy et al., 2018; Wünsch et al., 2019). PARAFAC was computed using two to nine component models, with non-negativity constraints and residual analysis, and split-half analysis was employed to validate the number of fluorescent components. Based on the results of the split-half and core consistency analyses, three-component models were chosen for further investigation. The relative contribution of individual chromophores was estimated by calculating the maximum fluorescence intensities (F_{max}: maximum fluorescence intensity of the identified fluorescent components; relative content (%) = $F_{max}/\Sigma F_{max}$) (Chen et al., 2020; Fan et al., 2020).

3. Results and discussion

3.1. Fluorescence properties of BrC model compounds

To identify whether the light-absorbing species possess fluorescence, a series of BrC model compounds were tested by the EEM method, and the fluorescence profiles are shown in Fig. S1. The results revealed that the location and intensity of the fluorescence peaks of different compounds were different, which varied with the distinct functional groups and aromatic conjugate system.

Although phenolic compounds are important light-absorbing species in atmospheric BrC (Smith et al., 2016; Yu et al., 2014, 2016), not all of them exhibit strong fluorescence. As shown in Fig. S1a, a strong fluorescence peak in the EEM spectrum of phenol was observed at Ex/Em = 270/295 nm. When the phenol

compounds were substituted with electron-donating groups (e.g., hydroxyl), all of the stronger fluorescence peaks were obviously red-shifted to 310–320 nm (e.g., catechol, hydroquinone, and 2-methoxyphenol). However, phenolic compounds substituted with electron-withdrawing groups (e.g., carboxyl and aldehyde) displayed weaker or even no fluorescence (Fig. S1a). These differences could be due to the ability of the electron-donating groups to form a larger conjugate system coupled with the benzene ring and decrease the $\pi \rightarrow \pi^*$ transition energy, thus leading to an increase in the Em wavelength (i.e., red shift) and variation in fluorescence intensity (Chen et al., 2002; Andrade-Eiroa et al., 2013). In contrast, the electron-withdrawing group can reduce the conjugated structure formed by the benzene ring and hydroxyl group, reducing the fluorescence intensity (Andrade-Eiroa et al., 2010; Andrade-Eiroa et al., 2013).

Aromatic acid and its derivatives are also important light-absorbing organic compounds in atmospheric BrC. Owing to the negative effects of the carboxyl group, a weak fluorescence peak (275/315 nm) was identified for benzoic acid, and no fluorescence was detected for benzene polycarboxylic acids, such as phthalic acid, terephthalic acid, and trimesic acid (Fig. S1b). However, when benzoic acid was substituted with electron-donating groups (e.g., hydroxyl, methoxy), higher intensity fluorescence peaks were observed. Two strong fluorescence peaks at 230/405 and 290/405 nm were identified for 2-hydroxybenzoic acid substituted with only one hydroxyl group. These peaks could have been the result of the ortho structure of the hydroxy and carboxyl groups, which is favorable for the formation of intramolecular

hydrogen bonds and generates a double-ring conjugate structure, reducing the transition energy and thereby presenting strong UV absorption and fluorescence (Andrade-Eiroa et al., 2013).

N-containing compounds, especially NACs, have strong light absorption, and have been reported to be the major components of atmospheric BrC, accounting for more than 60% of the total light absorption intensity at 300–500 nm (Huang et al., 2021; Lin et al., 2016; Lin et al., 2017; Wang et al., 2017; Frka et al, 2022). However, most of the NACs did not exhibit any fluorescence (Fig. S1c), similar to that reported in a previous study by Chen et al. (2020), which could be due to the significant reduction in the electron density of the benzene ring by the nitro ($-NO_2$) group—strong electron-withdrawing group—thereby weakening the fluorescence.

Tryptophan and tyrosine are the two most studied PRLIS species, and their EEM spectra are generally used as standards for comparison with fluorophores in atmospheric WSOM (Matos et al., 2015; Qin et al., 2018). As shown in Fig. S1d, the Ex/Em peaks at 275/300 and 275/350 nm corresponded to tyrosine and tryptophan, respectively. The maximum Em wavelength of phenylalanine was more inclined to short wavelength (280 nm) and with much weaker fluorescence intensity. Moreover, the fluorescence peaks of PRLIS obviously overlapped with those of phenols and aromatic acids (Fig. S1a, b). It must be noted that the concentrations of phenols and aromatic acids were significantly higher than those of tryptophan and tyrosine in the atmospheric samples (Table S2); therefore, the aerosol BrC fluorophores in these regions are more likely to have originated from phenols and aromatic acids rather

than PRLIS.

N-heterocyclic compounds such as pyrrole, pyridine, and imidazole are commonly identified in atmospheric samples (Dou et al., 2015; Jiang et al., 2019; Kosyakov et al., 2020). However, no fluorescence was observed for these three species in the present study, indicating that the absorbed energy may have been consumed by relaxation or vibration (Fig. S1e). Nevertheless, imidazole-2-formaldehyde produced two strong fluorescence peaks at 290/440 and 350/440 nm, formed from the oxidation of imidazole, suggesting that some N-heterocyclic compounds from secondary reactions may exhibit strong fluorescence at higher wavelength in atmospheric BrC (Ackendorf et al., 2017).

PAHs and their derivatives are mainly formed from incomplete combustion processes and are important components of BrC (Chen et al., 2020; Lin et al., 2017; Mahamuni et al., 2020). As shown in Fig. S1f, all PAHs exhibited strong fluorescence emission, with its peak location associated with the conjugated aromatic system. Naphthalene presented a fluorescence band located at the maximum Em wavelength of approximately 325 nm. As expected, with the increasing size of the π-bond system and degree of conjugation, the fluorescence band moved toward the longer wavelength range, and a new Em band was observed at 360–390 nm for 3–4-ring phenanthrene and pyrene, and at 400–500 nm for ≥ 5-ring PAHs (Mahamuni et al., 2020). The fluorescence spectra of high-ring PAHs were more complex because of more types of double bonds. As shown in Fig. S1f, the intensity and location of the fluorescence peaks were also significantly changed

when different types of groups were substituted with PAHs. For example, 1-naphthol exhibited a stronger EEM peak at a relatively longer wavelength (230, 290/460 nm) owing to its highly conjugated structure, when compared with naphthalene. This EEM spectrum was located in the EEM region of FAs, implying that FAs are composed of aromatic units and O-containing groups. In contrast, relatively weaker fluorescence was observed for 9-fluorenone, anthraquinone, and 2-naphthalenecarboxylic acid, and no EEM signals were observed for 2-nitronaphthol (Fig. S1c), which was substituted with a strong electron-withdrawing group ($–NO_2$).

3.2. Fluorescence properties of BrC from different sources

As shown in Fig. S4a and S4b, BB and CC WSOM exhibited similar fluorescence spectra (Tang et al., 2020a; Chen et al., 2020; Yang et al., 2022), with two types of fluorescence peaks at Ex/Em ≈ (230–240)/(340–400) nm (peak A) and Ex/Em ≈ (260–280)/(330–360) nm (peak B), respectively. The two fluorescence peaks were similar to those previously reported for BB WSOM and HULIS (Fan et al., 2020; Tang et al., 2020a; Yang et al., 2022). In general, peak A mainly corresponds to the protein-like UV region, with a minor contribution from fulvic-like substances, whereas peak B could be attributed to tryptophan-like fluorophores. However, based on the results of the present study, these two peaks could be mainly attributed to aromatic species such as aromatic acids, phenolic compounds, and minor quantities of PAHs (e.g., naphthalene) (Fig. 1). The fluorescence spectra of

WSOM from two types of vehicles (diesel and gasoline) also presented two fluorophores. A relatively strong fluorescence peak was observed at the low Ex wavelength (Ex/Em ≈ 230/350 nm) and a relatively weaker peak was detected at the high Ex wavelength (Ex/Em ≈ 270/350 nm) (Fig. S4c). These results are consistent with those reported in previous studies on VE (Chen et al., 2020; Tang et al., 2020a; Yang et al., 2022) and similar to the EEM fluorescence spectra of BB and CC WSOM (Chen et al., 2020; Fan et al., 2020; Cao et al., 2021; Yang et al., 2022). However, the fluorescence ranges of vehicle WSOM were obviously narrower, suggesting that BB and CC WSOM fluorescent components are more complex.

Soil-derived DOM is also a primary source of atmospheric WSOM. As shown in Fig. S5a, two main fluorescence peaks located at Ex/Em = 230/430 and 320/430 nm, were detected in the fluorescence spectra of soil DOM, which are similar to those reported in previous studies (Ge et al., 2021; Liu et al., 2009) and particularly close to the position of FAs (Fig. S5b).

Secondary chemical formation is another important source of atmospheric WSOM. For example, the aqueous-phase reactions of aldehydes with ammonium sulfate (AS) can produce highly fluorescent species (Hawkins et al., 2016). The Glyoxal-AS and glyoxal/glycine reaction products fluoresces at 340/450 nm, whereas formaldehyde-AS reaction product fluoresce at 250/430 nm. Secondary organic aerosols (SOAs) produced in the limonene/O_3 system have been reported to strongly fluoresce in the presence of NH_3 (Bones et al., 2010). In addition, aging of primary organic compounds has also been found to change the fluorescence spectra

(Lee et al., 2013; Li et al., 2021; Powelson et al., 2014). For instance, aging of syringic acid with OH radicals caused the initial fluorescence band to move toward the long wavelength range, producing a new band at a broad Em band at 400–600 nm. Similarly, the fluorescence peaks red-shifted (e.g., from 260–270/360 nm to 280–290/390–400 nm) during the O_3 aging process (Fan et al., 2020), suggesting the degradation of the initial compound and formation of new secondary organic compounds generally located at longer wavelengths, possibly with a high degree of aromaticity or highly oxidized functional groups (Chen et al., 2016a; Vidović et al., 2019, 2020; Powelson et al., 2014; Vione et al., 2019; Yu et al., 2016).

3.3. Identification of chemical species and potential sources of fluorescent components in ambient aerosols

The typical EEM spectra of atmospheric water-soluble light-absorbing compounds are shown in Fig. 2. Three fluorescence peaks were identified in the aerosol WSOM samples: a stronger fluorescence peak at Ex/Em = 230–250/360–420 nm, and two relatively weaker fluorescence peaks at Ex/Em = 270–290/340–370 nm and 300–320/360–420 nm. Similar fluorescence bands have been previously identified in the EEM fluorescence spectra of WSOM from $PM_{2.5}$ in the cold and warm seasons in Aveiro, Portugal (Matos et al., 2015), the High Arctic atmosphere (Fu et al., 2015), Godavari, Nepal (Wu et al., 2019), Lanzhou and Xi'an, northwestern China (Qin et al., 2018; Chen et al., 2020), Chongqing, southwestern China (Wang et al., 2020), and Harbin, northeastern China (Ma et al., 2022).

Although the fluorescence intensities varied with different sites and seasons, the shapes of the EEM spectra of WSOM were very similar, making it difficult to directly distinguish the different samples solely based on the characteristics of the EEM profiles. Therefore, a more powerful protocol named the PARAFAC method was employed to identify the individual fluorophores in ambient WSOM.

3.3.1. Identification and quantification of fluorescent components by the PARAFAC method

As shown in Fig. 3, three fluorescent components (C1, C2, and C3) were identified in the atmospheric samples; C1 occurred at a relatively lower Em wavelength, exhibiting two fluorescence peaks at Ex/Em = 235(270)/330 nm, C2 presented fluorescence peaks at around Ex/Em = 235(320)/390 nm, and C3 had a longer Em wavelength than C1 and C2, which was located at Ex/Em = about 250(355)/455 nm. In general, these fluorescent components have been interpreted based on knowledge of the fluorescence characteristics of aquatic DOM. Accordingly, C1 is considered to belong to the typical PRLIS (Coble, 1996; Wünsch et al., 2019), C2 is associated with fulvic-like substances or less-oxygenated HULIS (Liu et al., 2009; Zhang et al., 2014), and C3 is usually considered to correspond to terrestrial HULIS that are highly oxygenated organic matter (Table S3) (Liu et al., 2009; Wünsch et al., 2019; Zhou et al., 2017). However, it must be noted that the sources and transformation process are significantly different for WSOM in aerosols and DOM in aquatic and terrestrial environments; therefore, the fluorescence

classifications of DOM might not be applicable to atmospheric WSOM.

In general, the Ex and Em wavelengths of fluorescent components are mainly associated with their chemical characteristics and structures (Table S1 and Fig. 1). In the present study, C1 was similar to tryptophan-like fluorophores associated with PRLIS in rainwater (Zhang et al., 2014; Zhou et al., 2017) and fog water (Bianco et al., 2014; Bianco et al., 2016). However, this fluorophore might also be related to small molecular aromatic compounds, such as aromatic acids (e.g., 3,5-dihydroxybenzoic acid and 2-naphthalenecarboxylic acid) and PAHs (e.g., naphthalene, phenanthrene, and anthraquinone) (Fig. 1a) (Miyakawa et al., 2015; Wu et al., 2019). In addition, this fluorophore could also contain traces of some phenolic compounds, including catechol, hydroquinone, and 2-methoxyphenol. These organic species might be generated by various types of combustion processes and atmospheric oxidation reactions. It must be noted that investigations of the fluorescent components in atmospheric WSOM should not only consider their position in the fluorescence spectrum, but also their concentration and possibility of trapping. Many previous studies have reported that the concentration of amino acids in atmospheric aerosols is almost negligible, when compared with that of lower molecular weight aromatic compounds such as aromatic acids and phenolic compounds (Table S2) (Bianco et al., 2016; Song et al., 2017; Vione et al., 2019; Mahamuni et al., 2020; and references therein). Therefore, fluorescent components in this Ex/Em region could be attributed to small molecular aromatic species (e.g, aromatic acids, phenolic compounds) rather than PRLIS. Moreover, this fluorophore

371 overlapped with that of WSOM from combustion process such as BB, CC, and VE
372 (Fig. 1b), suggesting significant contribution of the combustion process.

373 When compared with C1, C2 exhibited a strong fluorescence peak at longer
374 Ex/Em wavelength of 235(320)/390 nm, implying that this fluorescent component
375 presented a relatively larger molecular size and higher aromaticity than C1 (Pöhlker
376 et al., 2012). As shown in Fig. 1a, the fluorescence of C2 is similar to that of
377 aromatic compounds (e.g., 2-naphthalenecarboxylic acid, 2-hydroxybenzoic acid,
378 anthraquinone) and high-ring PAHs (e.g., pyrene, anthraquinone, anthracene,
379 chrysene) (Mahamuni et al., 2020), and overlaps with the fluorescence spectra of
380 FAs. In addition, this fluorophore has also been reported to be related to the
381 generation of SOAs from organic precursors emitted from biological/anthropogenic
382 emission and combustion processes (Wang et al., 2020). For example, the
383 aqueous-phase reactions of aldehydes with AS have been proposed as an important
384 source of atmospheric BrC, which present similar fluorescence spectral profiles
385 (Hawkins et al., 2016; Lee et al., 2013) (Fig. 1b). In addition, oxidative
386 oligomerization of phenols and their derivatives can also shift the Ex/Em wavelength
387 of these substances to longer wavelengths, falling into similar fluorescence regions
388 (Li et al., 2021; Tang et al., 2020a; Vione et al., 2019). As suggested by Chen et al.
389 (2016a), this fluorescent component may be a less-oxygenated fluorescent group
390 contributed by biomass combustion. Therefore, fluorophore C2 might be related to
391 the derivatives of biomass burning and/or biogenic molecules, with relatively lower
392 degree of oxidation (Chen et al., 2016a; Jiang et al., 2022).

C3 presented a longer Em wavelength than C1 and C2, with two peaks at around Ex/Em=250/455 nm and 355/455 nm (Fig. 3). This fluorescent component overlaps with the fluorescence of high-ring PAHs and their derivatives, such as fluoranthene, benzo-b-fluoranthene, benzo-a-pyrene, indeno-123cd-pyrene, 1-naphthol, and N-heterocyclic compounds, including imidazole-2-formaldehyde (Chen et al., 2020; Mahamuni et al., 2020). Furthermore, this fluorescent component exhibited a similar Ex/Em wavelength to that of FAs and HAs (Fig. S5b), suggesting the possible contribution of soil dust, and thus could be assigned as HULIS (Lin and Guo, 2020). Similar fluorescent substances have also been identified in the study of atmospheric aerosol fluorescent chromophores, such as the highly oxygenated HULIS in Nagoya, Japan (Chen et al., 2016a), Lanzhou, China (Qin et al., 2018), Xi'an, China (Chen et al., 2020), a haze event in Harbin (Ma et al., 2022), and humic-like compounds with more aromatic and unsaturated bonds in Godavari, Nepal (Wu et al., 2019) and Tianjin, China(Deng et al., 2022). Based on the PARAFAC results with aerosol mass spectrometry data, C3 was considered to be a fluorescent group with high oxygen content and high O/C ratio, close to that of aged organic aerosols (Chen et al., 2016a; Jiang et al., 2022) (Fig. 1b). It must be noted that low molecular weight organic compounds can further undergo oligomerization to high molecular weight species with long Em wavelengths during the aging process (Hawkins et al., 2016; Li et al., 2021; Tang et al., 2020b; Yu et al., 2016). The resulting compounds may present a more complex structure than their precursor, probably owing to the presence of condensed aromatic rings and other π-electron

systems with a high level of conjugation; thus, atmospheric aging is assumed to be a potential contributor to C3 (Barsotti et al., 2016; De Laurentiis et al., 2013; Hawkins et al., 2016).

3.3.2. Spatial and seasonal variations in fluorescent components in WSOM

The relative contributions of C1, C2, and C3 components to the total fluorescence intensities ($F_{max}/\sum F_{max}$) were calculated (Fig. 4), and were found to be similar for WSOM from CZ and GZ, exhibiting maximum C2 content and relatively lower C1 and C3 contents. Furthermore, WSOM samples showed obvious spatial and seasonal variations, similar to the results reported in other regions in China (Zhang et al., 2022a, 2022b). First, CZ WSOM presented a relatively higher C3 content (23±4%) than GZ WSOM (17±3%), whereas GZ WSOM had a relatively higher C2 content (56±7%) than CZ WSOM (49±4%) during the same sampling period. Such differences in the composition of fluorescent components may be ascribed to the variation in the primary emission sources and atmospheric aging process at the two sites. The relatively higher C3 content in the CZ could be attributed to the comparatively high contribution of soil dust in the suburban region, which is consistent with the relatively higher Ca^{2+} contents in the CZ $PM_{2.5}$ (1.8±1.2%) than in the GZ $PM_{2.5}$ (1.5±0.8%) (Vasilatou et al., 2017; Wu et al., 2019). In contrast, the relatively higher C2 content in GZ WSOM may be attributed to the comparatively stronger atmospheric chemical reaction associated with bio-volatile organic compounds (bio-VOCs) in the hot and humid region of GZ. This result was

consistent with the relatively higher humification index (HIX) and normalized fluorescence volume (NFV) values (log(NFV)) of CZ WSOM (Fig. S6) (Chen et al., 2020; Yang et al., 2022).

In addition, the resolved Ex and Em spectra for GZ WSOM were also similar in different seasons, implying that the types of fluorophores contributing to WSOM were predominantly the same throughout the year. However, the compositions of fluorescent components varied in different seasons. In the dry season (October–March), WSOM showed relatively higher contents of C3 fluorophores (17±4%), whereas in the wet season (April–September), slightly higher contents of C2 fluorophores (69±4%) were detected (Fig. 4) (Chen et al., 2020; Wang et al., 2020). These differences might be associated with the variations in the source composition and aging effects of BrC in different seasons. The higher content of C3 in WSOM in the dry season suggested the occurrence of more highly aromatic and highly oxidized compounds. These results could be explained by the fact that more aged organic aerosols and dust were transported from the northern region of China (Jiang et al., 2021). In contrast, the slightly higher C2 content in the wet season may be attributed to the relatively stronger secondary formation of bio-SOAs and photodegradation effects in the high-temperature and relative humidity season.

4. Conclusion and future prospects

In this study, the fluorescence properties of BrC model compounds were investigated to determine the chromophoric species that can be evaluated by the

EEM method. Accordingly, the aerosol WSOM samples at two sites (CZ and GZ) were investigated by the EEM-PARAFAC method, and the chemical characteristics and potential sources of fluorescent components were examined. The main conclusions and future prospects are as follows:

(1) Fluorescent components have predominantly been evaluated based on the knowledge of fluorophores in aquatic DOM, which often leads to misinterpretation. In the present study, the chemical characteristics of fluorophores in different Ex/Em regions were discussed based on the fluorescence properties of BrC model compounds and their amounts in aerosols. In particular, the C1 fluorophore in atmospheric WSOM, which has been frequently assigned to PRLIS because of the similarity in fluorescence spectra, was demonstrated to mainly include aromatic acids, phenolic compounds, and their derivatives, with negligible amounts of amino acids.

(2) The fluorescence properties of target compounds are mainly influenced by the aromatic system and characteristics of adjacent functional groups. Organic compounds with high aromaticity and strong electron-donating groups (e.g., hydroxyl, methoxyl) generally exhibited strong fluorescence spectra at longer Em wavelengths, whereas organic compounds substituted with electron-withdrawing groups presented relatively weaker fluorescence intensities. In particular, aromatic compounds containing nitro groups (i.e., nitrophenols) showed strong absorption and were the major component of atmospheric BrC; however, they did not exhibit significant fluorescene. Thus, the fluorescence method could only measure a subset

of chromophores in aerosol BrC and should be used with caution for the investigation of aerosol BrC.

(3) The EEM spectra for aerosol WSOM were very similar; however, the relative contents of certain fluorescent components significantly varied with the sampling site and season. For example, more fluorescent components associated with soil and secondary oxidation of small molecular compounds from combustion emission were identified in CZ WSOM, whereas more fluorescent components derived from atmospheric chemical reaction of bio-VOCs were observed in GZ WSOM. In addition, GZ WSOM exhibited more highly aromatic and highly oxidized compounds in the dry season.

Although many studies have applied the EEM-PARAFAC method to investigate atmospheric WSOM and have obtained useful data, there are still challenges and gaps that must be addressed. First, caution should be taken for credible interpretations of the fluorescent components in atmospheric WSOM because of the differences in chemical characteristics of organic matter derived from different sources. In addition, the same fluorophores may exhibit different Ex/Em ranges and intensities in different environmental conditions (e.g., pH, coexisting metal ions and inorganic salts). Therefore, more theoretical and experimental studies are necessary to understand the relationship between the fluorescent groups and positions of fluorescence peaks, as well as the influences of sources and chemical formation process of the fluorescent groups on fluorescence peaks.

Data availability

The research data can be accessed in the Harvard Dataverse (https://doi.org/10.7910/DVN/ULCIU9, Song, 2022)

Author contributions. J. Song designed the research. T. Cao and C. Xu, analyzed the model compounds and WSOM samples by UV-Vis and EEM. T. Cao and X. Fan resolved the EEM by PARAFAC tool. M. Li carried out the $PM_{2.5}$ sampling experiments. T. Cao and J. Song wrote the paper. J. Li, W. Jia, and P. Peng commented and revised the paper.

Competing interests. The authors declare that they have no conflict of interest

Acknowledgments. The present work was supported by the National Natural Science Foundation of China (42192514 and 41977188), Guangdong Foundation for Program of Science and Technology Research (2020B1212060053), and Guangdong Foundation for Program of Science and Technology Research (2019B121205006).

References

Ackendorf, J. M., Ippolito, M. G., and Galloway, M. M.: pH Dependence of the Imidazole-2-carboxaldehyde Hydration Equilibrium: Implications for Atmospheric Light Absorbance, Environ. Sci. Technol. Let., 4, 551-555, http://doi.org/10.1021/acs.estlett.7b00486, 2017.

525 Aftab, B., Shin, H. S., and Hur, J.: Exploring the fate and oxidation behaviors of
526 different organic constituents in landfill leachate upon Fenton oxidation
527 processes using EEM-PARAFAC and 2D-COS-FTIR, J. Haza. Mat., 354, 33-41,
528 http://doi.org/10.1016/j.jhazmat.2018.04.059, 2018.
529 Andrade-Eiroa, A., Leroy, V., and Dagaut, P.: Advances in PAHs/nitro-PAHs
530 fractioning, Anal. Meth., 2, 2017, http://doi.org/10.1039/c0ay00484g, 2010.
531 Andrade-Eiroa, Á., Canle, M., and Cerdá, V.: Environmental Applications of
532 Excitation-Emission Spectrofluorimetry: An In-Depth Review I, Appl. Spec.
533 Rev., 48, 1-49, http://doi.org/10.1080/05704928.2012.692104, 2013.
534 Barsotti, F., Ghigo, G., and Vione, D.: Computational assessment of the fluorescence
535 emission of phenol oligomers: A possible insight into the fluorescence
536 properties of humic-like substances (HULIS), J. Photo. Photo. A., 315, 87-93,
537 http://doi.org/10.1016/j.jphotochem.2015.09.012, 2016.
538 Bianco, A., Minella, M., De Laurentiis, E., Maurino, V., Minero, C., and Vione, D.:
539 Photochemical generation of photoactive compounds with fulvic-like and
540 humic-like fluorescence in aqueous solution, Chemosphere, 111, 529-536,
541 http://doi.org/10.1016/j.chemosphere.2014.04.035, 2014.
542 Bianco, A., Passananti, M., Deguillaume, L., Mailhot, G., and Brigante, M.:
543 Tryptophan and tryptophan-like substances in cloud water: Occurrence and
544 photochemical fate, Atmos. Environ., 137, 53-61,
545 http://doi.org/10.1016/j.atmosenv.2016.04.034, 2016.

546 Bones, D. L., Henricksen, D. K., Mang, S. A., Gonsior, M., Bateman, A. P., Nguyen,
547 T. B., Cooper, W. J., and Nizkorodov, S. A.: Appearance of strong absorbers and
548 fluorophores in limonene-O_3 secondary organic aerosol due to $NH4^+$-mediated
549 chemical aging over long time scales, J. Geophys. Res.-Atmos., 115, D05203,
550 http://doi.org/10.1029/2009jd012864, 2010.
551 Cao, T., Li, M. J., Zou, C. L., Fan, X. J., Song, J. Z., Jia, W. L., Yu, C. L., Yu, Z. Q.,
552 and Ping, P. A.: Chemical composition, optical properties, and oxidative
553 potential of water- and methanol-soluble organic compounds emitted from the
554 combustion of biomass materials and coal, Atmos. Chem. Phys., 21,
555 13187-13205, http://doi.org/10.5194/acp-21-13187-2021, 2021.
556 Chen, J., Gu, B. H., LeBoeuf, E. J., Pan, H. J., and Dai, S.: Spectroscopic
557 characterization of the structural and functional properties of natural organic
558 matter fractions, Chemosphere, 48, 59-68,
559 https://doi.org/10.1016/s0045-6535(02)00041-3, 2002.
560 Chen, Q., Ikemori, F., and Mochida, M.: Light Absorption and Excitation-Emission
561 Fluorescence of Urban Organic Aerosol Components and Their Relationship to
562 Chemical Structure, Environ. Sci. Technol., 50, 10859-10868,
563 http://doi.org/10.1021/acs.est.6b02541, 2016a.
564 Chen, Q., Miyazaki, Y., Kawamura, K., Matsumoto, K., Coburn, S., Volkamer, R.,
565 Iwamoto, Y., Kagami, S., Deng, Y., Ogawa, S., Ramasamy, S., Kato, S., Ida, A.,
566 Kajii, Y., and Mochida, M.: Characterization of Chromophoric Water-Soluble
567 Organic Matter in Urban, Forest, and Marine Aerosols by HR-ToF-AMS

568 Analysis and Excitation-Emission Matrix Spectroscopy, Environ. Sci. Technol.,
569 50, 10351-10360, http://doi.org/10.1021/acs.est.6b01643, 2016b.
570 Chen, Q., Li, J., Hua, X., Jiang, X., Mu, Z., Wang, M., Wang, J., Shan, M., Yang, X.,
571 Fan, X., Song, J., Wang, Y., Guan, D., and Du, L.: Identification of species and
572 sources of atmospheric chromophores by fluorescence excitation-emission
573 matrix with parallel factor analysis, Sci. Total Environ., 718, 137322,
574 http://doi.org/10.1016/j.scitotenv.2020.137322, 2020.
575 Coble, P. G.: Characterization of marine and terrestrial DOM in seawater using
576 excitation emission matrix spectroscopy, Marin. Chem., 51, 325-346,
577 http://doi.org/10.1016/0304-4203(95)00062-3, 1996.
578 Coble, P. G.: Marine optical biogeochemistry: The chemistry of ocean color, Chem.
579 Rev., 107, 402-418, http://doi.org/10.1021/cr050350+, 2007.
580 De Laurentiis, E., Maurino, V., Minero, C., Vione, D., Mailhot, G., and Brigante, M.:
581 Could triplet-sensitised transformation of phenolic compounds represent a
582 source of fulvic-like substances in natural waters?, Chemosphere, 90, 881-884,
583 http://doi.org/10.1016/j.chemosphere.2012.09.031, 2013.
584 Deng, J., Ma, H., Wang, X., Zhong, S., Zhang, Z., Zhu, J., Fan, Y., Hu, W., Wu, L.,
585 Li, X., Ren, L., Pavuluri, C. M., Pan, X., Sun, Y., Wang, Z., Kawamura, K., and
586 Fu, P.: Measurement report: Optical properties and sources of water-soluble
587 brown carbon in Tianjin, North China – insights from organic molecular
588 compositions, Atmos. Chem. Phys., 22, 6449-6470,
589 https://doi.org/10.5194/acp-22-6449-2022, 2022.

590 Dou, J., Lin, P., Kuang, B. Y., and Yu, J. Z.: Reactive Oxygen Species Production
591 Mediated by Humic-like Substances in Atmospheric Aerosols: Enhancement
592 Effects by Pyridine, Imidazole, and Their Derivatives, Environ. Sci. Technol.,
593 49, 6457-6465, http://doi.org/10.1021/es5059378, 2015.
594 Fan, X., Cao, T., Yu, X., Wang, Y., Xiao, X., Li, F., Xie, Y., Ji, W., Song, J., Peng, P.,
595 amp, apos, and an: The evolutionary behavior of chromophoric brown carbon
596 during ozone aging of fine particles from biomass burning, Atmos. Chem. Phys.,
597 20, 4593-4605, http://doi.org/10.5194/acp-20-4593-2020, 2020.
598 Frka, S., Šala, M., Brodnik, H., Štefane, B., Kroflič, A., and Grgić, I.: Seasonal
599 variability of nitroaromatic compounds in ambient aerosols: Mass size
600 distribution, possible sources and contribution to water-soluble brown carbon
601 light absorption, Chemosphere, 299, 134381,
602 https://doi.org/10.1016/j.chemosphere.2022.134381, 2022.
603 Fu, P., Kawamura, K., Chen, J., Qin, M., Ren, L., Sun, Y., Wang, Z., Barrie, L. A.,
604 Tachibana, E., Ding, A., and Yamashita, Y.: Fluorescent water-soluble organic
605 aerosols in the High Arctic atmosphere, Sci. Rep., 5, 9845,
606 http://doi.org/10.1038/srep09845, 2015.
607 Ge, Z., Gao, L., Ma, N., Hu, E., and Li, M.: Variation in the content and fluorescent
608 composition of dissolved organic matter in soil water during rainfall-induced
609 wetting and extract of dried soil, Sci. Total Environ., 791, 148296,
610 http://doi.org/10.1016/j.scitotenv.2021.148296, 2021.

611 Graber, E. R., and Rudich, Y.: Atmospheric HULIS: How humic-like are they? A
612 comprehensive and critical review, Atmos. Chem. Phys., 6, 729-753,
613 http://doi.org/10.5194/acp-6-729-2006, 2006.
614 Hawkins, L. N., Lemire, A. N., Galloway, M. M., Corrigan, A. L., Turley, J. J.,
615 Espelien, B. M., and De Haan, D. O.: Maillard Chemistry in Clouds and
616 Aqueous Aerosol As a Source of Atmospheric Humic-Like Substances, Environ.
617 Sci. Technol., 50, 7443-7452, http://doi.org/10.1021/acs.est.6b00909, 2016.
618 Huang, R.-J., Yang, L., Shen, J., Yuan, W., Gong, Y., Ni, H., Duan, J., Yan, J., Huang,
619 H., You, Q., and Li, Y. J.: Chromophoric Fingerprinting of Brown Carbon from
620 Residential Biomass Burning, Environ. Sci. Technol. Let., 9, 102-111,
621 http://doi.org/10.1021/acs.estlett.1c00837, 2021.
622 Huang, S., Luo, Y., Wang, X., Zhang, T., Lei, Y., Zeng, Y., Sun, J., Che, H., Xu, H.,
623 Cao, J., and Shen, Z.: Optical properties, chemical functional group, and
624 oxidative activity of different polarity levels of water-soluble organic matter in
625 PM2.5 from biomass and coal combustion in rural areas in Northwest China,
626 Atmos. Environ., 283, 119179, https://doi.org/10.1016/j.atmosenv.2022.119179,
627 2022.
628 Huo, Y. Q., Li, M., Jiang, M. H., and Qi, W. M.: Light absorption properties of
629 HULIS in primary particulate matter produced by crop straw combustion under
630 different moisture contents and stacking modes, Atmos. Environ., 191,
631 490-499, http://doi.org/10.1016/j.atmosenv.2018.08.038, 2018.

Jiang, H., Frie, A. L., Lavi, A., Chen, J. Y., Zhang, H., Bahreini, R., and Lin, Y.-H.: Brown Carbon Formation from Nighttime Chemistry of Unsaturated Heterocyclic Volatile Organic Compounds, Environ. Sci. Technol. Let., 6, 184-190, http://doi.org/10.1021/acs.estlett.9b00017, 2019.

Jiang, H., Tang, J., Li, J., Zhao, S., Mo, Y., Tian, C., Zhang, X., Jiang, B., Liao, Y., Song, J., Chen, Y., Zhang, G., 2022. Molecular Signatures of Fluorescence Components in Atmospheric Organic Matters Inferred from Positive and Negative Electrospray Ionization Fourier Transform Ion Cyclotron Resonance Mass Spectrometry. Environ. Sci. Technol. Let., 9, 11, 913-920., https://doi.org/10.1021/acs.estlett.2c00629, 2022.

Jiang, H. X., Li, J., Sun, R., Liu, G. Q., Tian, C. G., Tang, J., Cheng, Z. N., Zhu, S. Y., Zhong, G. C., Ding, X., and Zhang, G.: Determining the Sources and Transport of Brown Carbon Using Radionuclide Tracers and Modeling, J. Geophys. Res.-Atmos., 126, e2021JD034616, http://doi.org/10.1029/2021JD034616, 2021.

Kosyakov, D. S., Ul'yanovskii, N. V., Latkin, T. B., Pokryshkin, S. A., Berzhonskis, V. R., Polyakova, O. V., and Lebedev, A. T.: Peat burning – An important source of pyridines in the earth atmosphere, Environ. Pollut., 266, 115109, http://doi.org/10.1016/j.envpol.2020.115109, 2020.

Laskin, A., Laskin, J., and Nizkorodov, S. A.: Chemistry of atmospheric brown carbon, Chem. Rev., 115, 4335-4382, http://doi.org/10.1021/cr5006167, 2015.

Lee, H. J., Laskin, A., Laskin, J., and Nizkorodov, S. A.: Excitation-emission spectra and fluorescence quantum yields for fresh and aged biogenic secondary organic aerosols, Environ. Sci. Technol., 47, 5763-5770, http://doi.org/10.1021/es400644c, 2013.

Li, F., Tsona, N. T., Li, J., and Du, L.: Aqueous-phase oxidation of syringic acid emitted from biomass burning: Formation of light-absorbing compounds, Sci. Total Environ., 765, 144239, http://doi.org/10.1016/j.scitotenv.2020.144239, 2021.

Lin, H., and Guo, L.: Variations in Colloidal DOM Composition with Molecular Weight within Individual Water Samples as Characterized by Flow Field-Flow Fractionation and EEM-PARAFAC Analysis, Environ. Sci. Technol., 54, 1657-1667, http://doi.org/10.1021/acs.est.9b07123, 2020.

Lin, P., Aiona, P. K., Li, Y., Shiraiwa, M., Laskin, J., Nizkorodov, S. A., and Laskin, A.: Molecular Characterization of Brown Carbon in Biomass Burning Aerosol Particles, Environ. Sci. Technol., 50, 11815-11824, http://doi.org/10.1021/acs.est.6b03024, 2016.

Lin, P., Bluvshtein, N., Rudich, Y., Nizkorodov, S. A., Laskin, J., and Laskin, A.: Molecular Chemistry of Atmospheric Brown Carbon Inferred from a Nationwide Biomass Burning Event, Environ. Sci. Technol., 51, 11561-11570, http://doi.org/10.1021/acs.est.7b02276, 2017.

Liu, L., Song, C., Yan, Z., and Li, F.: Characterizing the release of different composition of dissolved organic matter in soil under acid rain leaching using

three-dimensional excitation-emission matrix spectroscopy, Chemosphere, 77, 15-21, http://doi.org/10.1016/j.chemosphere.2009.06.026, 2009.

Ma, L., Li, B., Yabo, S. D., Li, Z., and Qi, H.: Fluorescence fingerprinting characteristics of water-soluble organic carbon from size-resolved particles during pollution event, Chemosphere, 307, 135748, https://doi.org/10.1016/j.chemosphere.2022.135748, 2022.

Mahamuni, G., Rutherford, J., Davis, J., Molnar, E., Posner, J. D., Seto, E., Korshin, G., and Novosselov, I.: Excitation–Emission Matrix Spectroscopy for Analysis of Chemical Composition of Combustion Generated Particulate Matter, Environ. Sci. Technol., 54, 8198-8209, http://doi.org/10.1021/acs.est.0c01110, 2020.

Matos, J. T. V., Freire, S. M. S. C., Duarte, R. M. B. O., and Duarte, A. C.: Natural organic matter in urban aerosols: Comparison between water and alkaline soluble components using excitation-emission matrix fluorescence spectroscopy and multiway data analysis, Atmos. Environ., 102, 1-10, http://doi.org/10.1016/j.atmosenv.2014.11.042, 2015.

Miyakawa, T., Kanaya, Y., Taketani, F., Tabaru, M., Sugimoto, N., Ozawa, Y., and Takegawa, N.: Ground-based measurement of fluorescent aerosol particles in Tokyo in the spring of 2013: Potential impacts of nonbiological materials on autofluorescence measurements of airborne particles, J. Geophys. Res.-Atmos., 120, 1171-1185, http://doi.org/10.1002/2014jd022189, 2015.

Murphy, K. R., Butler, K. D., Spencer, R. G. M., Stedmon, C. A., Boehme, J. R., and Aiken, G. R.: Measurement of Dissolved Organic Matter Fluorescence in

Aquatic Environments: An Interlaboratory Comparison, Environ. Sci. Technol., 44, 9405-9412, http://doi.org/10.1021/es102362t, 2010.

Murphy, K. R., Stedmon, C. A., Graeber, D., and Bro, R.: Fluorescence spectroscopy and multi-way techniques. PARAFAC, Anal. Meth., 5, 6557, http://doi.org/10.1039/c3ay41160e, 2013.

Murphy, K. R., Timko, S. A., Gonsior, M., Powers, L. C., Wünsch, U. J., and Stedmon, C. A.: Photochemistry Illuminates Ubiquitous Organic Matter Fluorescence Spectra, Environ. Sci. Technol., 52, 11243-11250, http://doi.org/10.1021/acs.est.8b02648, 2018.

Niu, X., Pu, W., Fu, P., Chen, Y., Xing, Y., Wu, D., Chen, Z., Shi, T., Zhou, Y., Wen, H., and Wang, X.: Fluorescence characteristics, absorption properties, and radiative effects of water-soluble organic carbon in seasonal snow across northeastern China, Atmos. Chem. Phys., 22, 14075-14094, https://doi.org/10.5194/acp-22-14075-2022, 2022.

Pöhlker, C., Huffman, J. A., and Pöschl, U.: Autofluorescence of atmospheric bioaerosols – fluorescent biomolecules and potential interferences, Atmos. Meas. Tech., 5, 37-71, http://doi.org/10.5194/amt-5-37-2012, 2012.

Powelson, M. H., Espelien, B. M., Hawkins, L. N., Galloway, M. M., and De Haan, D. O.: Brown carbon formation by aqueous-phase carbonyl compound reactions with amines and ammonium sulfate, Environ. Sci. Technol., 48, 985-993, http://doi.org/10.1021/es4038325, 2014.

718 Qin, J., Zhang, L., Zhou, X., Duan, J., Mu, S., Xiao, K., Hu, J., and Tan, J.:
719 Fluorescence fingerprinting properties for exploring water-soluble organic
720 compounds in $PM_{2.5}$ in an industrial city of northwest China, Atmos. Environ.,
721 184, 203-211, http://doi.org/10.1016/j.atmosenv.2018.04.049, 2018.
722 Smith, J. D., Kinney, H., and Anastasio, C.: Phenolic carbonyls undergo rapid
723 aqueous photodegradation to form low-volatility, light-absorbing products,
724 Atmos. Environ., 126, 36-44, http://doi.org/10.1016/j.atmosenv.2015.11.035,
725 2016.
726 Song, J.: Data for CT, Harvard Dataverse [data set], (https://
727 doi.org/10.7910/DVN/ULCIU9, 2022.
728 Song, T., Wang, S., Zhang, Y., Song, J., Liu, F., Fu, P., Shiraiwa, M., Xie, Z., Yue, D.,
729 Zhong, L., Zheng, J., and Lai, S.: Proteins and Amino Acids in Fine Particulate
730 Matter in Rural Guangzhou, Southern China: Seasonal Cycles, Sources, and
731 Atmospheric Processes, Environ. Sci. Technol., 51, 6773-6781,
732 https://doi.org/10.1021/acs.est.7b00987, 2017.
733 Tang, J., Li, J., Su, T., Han, Y., Mo, Y., Jiang, H., Cui, M., Jiang, B., Chen, Y., Tang,
734 J., Song, J., Peng, P. a., and Zhang, G.: M.olecular compositions and optical
735 properties of dissolved brown carbon in biomass burning, coal combustion, and
736 vehicle emission aerosols illuminated by excitation–emission matrix
737 spectroscopy and Fourier transform ion cyclotron resonance mass spectrometry
738 analysis, Atmos. Chem. Phys., 20, 2513-2532,
739 http://doi.org/10.5194/acp-20-2513-2020, 2020a.

740 Tang, J., Wang, J., Zhong, G., Jiang, H., Mo, Y., Zhang, B., Geng, X., Chen, Y., Tang,
741 J., Tian, C., Bualert, S., Li, J., and Zhang, G.: Measurement report:
742 Long-emission-wavelength chromophores dominate the light absorption of
743 brown carbon in aerosols over Bangkok: impact from biomass burning, Atmos.
744 Chem. Phys., 21, 11337-11352, http://doi.org/10.5194/acp-21-11337-2021,
745 2021.
746 Tang, S., Li, F., Tsona, N. T., Lu, C., Wang, X., and Du, L.: Aqueous-Phase
747 Photooxidation of Vanillic Acid: A Potential Source of Humic-Like Substances
748 (HULIS), ACS Earth Space Chem., 4, 862-872,
749 http://doi.org/10.1021/acsearthspacechem.0c00070, 2020b.
750 Vasilatou, V., Diapouli, E., Abatzoglou, D., Bakeas, E. B., Scoullos, M., and
751 Eleftheriadis, K.: Characterization of $PM_{2.5}$ chemical composition at the
752 Demokritos suburban station, in Athens Greece. The influence of Saharan dust,
753 Environ. Sci. Pollut. Res., 24, 11836-11846,
754 https://doi.org/10.1007/s11356-017-8684-3, 2017.
755 Vidović, K., Kroflič, A., Jovanovič, P., Šala, M., and Grgić, I.: Electrochemistry as a
756 Tool for Studies of Complex Reaction Mechanisms: The Case of the
757 Atmospheric Aqueous-Phase Aging of Catechols, Environ. Sci. Technol., 53,
758 11195-11203, https://doi.org/10.1021/acs.est.9b02456, 2019.
759 Vidović, K., Kroflič, A., Šala, M., and Grgić, I.: Aqueous-Phase Brown Carbon
760 Formation from Aromatic Precursors under Sunlight Conditions, Atmosphere,
761 11, 131, https://doi.org/10.3390/atmos11020131, 2020.

762 Vione, D., Albinet, A., Barsotti, F., Mekic, M., Jiang, B., Minero, C., Brigante, M.,
763 and Gligorovski, S.: Formation of substances with humic-like fluorescence
764 properties, upon photoinduced oligomerization of typical phenolic compounds
765 emitted by biomass burning, Atmos. Environ., 206, 197-207,
766 http://doi.org/10.1016/j.atmosenv.2019.03.005, 2019.
767 Wünsch, U. J., Bro, R., Stedmon, C. A., Wenig, P., and Murphy, K. R.: Emerging
768 patterns in the global distribution of dissolved organic matter fluorescence, Anal.
769 Meth., 11, 888-893, http://doi.org/10.1039/c8ay02422g, 2019.
770 Wang, H., Zhang, L., Huo, T., Wang, B., Yang, F., Chen, Y., Tian, M., Qiao, B., and
771 Peng, C.: Application of parallel factor analysis model to decompose
772 excitation-emission matrix fluorescence spectra for characterizing sources of
773 water-soluble brown carbon in $PM_{2.5}$, Atmos. Environ., 223, 117192,
774 http://doi.org/10.1016/j.atmosenv.2019.117192, 2020.
775 Wozniak, A. S., Bauer, J. E., and Dickhut, R. M.: Characteristics of water-soluble
776 organic carbon associated with aerosol particles in the eastern United States,
777 Atmos. Environ., 46, 181-188, https://doi.org/10.1016/j.atmosenv.2011.10.001,
778 2012.
779 Wu, G., Ram, K., Fu, P., Wang, W., Zhang, Y., Liu, X., Stone, E. A., Pradhan, B. B.,
780 Dangol, P. M., Panday, A. K., Wan, X., Bai, Z., Kang, S., Zhang, Q., and Cong,
781 Z.: Water-Soluble Brown Carbon in Atmospheric Aerosols from Godavari
782 (Nepal), a Regional Representative of South Asia, Environ. Sci. Technol., 53,
783 3471-3479, http://doi.org/10.1021/acs.est.9b00596, 2019.

784 Wu, G., Fu, P., Ram, K., Song, J., Chen, Q., Kawamura, K., Wan, X., Kang, S.,
785 Wang, X., Laskin, A., and Cong, Z.: Fluorescence characteristics of
786 water-soluble organic carbon in atmospheric aerosol, Environ. Pollut., 268,
787 115906, http://doi.org/10.1016/j.envpol.2020.115906, 2020.
788 Wu, L., Luo, X.-S., Li, H., Cang, L., Yang, J., Yang, J., Zhao, Z., and Tang, M.:
789 Seasonal Levels, Sources, and Health Risks of Heavy Metals in Atmospheric
790 $PM_{2.5}$ from Four Functional Areas of Nanjing City, Eastern China, Atmosphere,
791 10, 419, https://doi.org/10.3390/atmos10070419, 2019.
792 Yan, G., and Kim, G.: Speciation and Sources of Brown Carbon in Precipitation at
793 Seoul, Korea: Insights from Excitation-Emission Matrix Spectroscopy and
794 Carbon Isotopic Analysis, Environ. Sci. Technol., 51, 11580-11587,
795 http://doi.org/10.1021/acs.est.7b02892, 2017.
796 Yang, Y., Qin, Y., Qin, J., Zhou, X., Xv, P., Tan, J., and Xiao, K.: Facile
797 Differentiation of Four Sources of Water-Soluble Organic Carbon in
798 Atmospheric Particulates Using Multiple Fluorescence Spectral Fingerprints,
799 Environ. Sci. Technol. Let., 9, 359-365,
800 http://doi.org/10.1021/acs.estlett.2c00128, 2022.
801 Yu, L., Smith, J., Laskin, A., Anastasio, C., Laskin, J., and Zhang, Q.: Chemical
802 characterization of SOA formed from aqueous-phase reactions of phenols with
803 the triplet excited state of carbonyl and hydroxyl radical, Atmos. Chem. Phys.,
804 14, 13801-13816, http://doi.org/10.5194/acp-14-13801-2014, 2014.

Yu, L., Smith, J., Laskin, A., George, K. M., Anastasio, C., Laskin, J., Dillner, A. M., and Zhang, Q.: Molecular transformations of phenolic SOA during photochemical aging in the aqueous phase: competition among oligomerization, functionalization, and fragmentation, Atmos. Chem. Phys., 16, 4511-4527, http://doi.org/10.5194/acp-16-4511-2016, 2016.

Zhang, T., Shen, Z. X., Zeng, Y. L., Cheng, C. L., Wang, D. W., Zhang, Q., Lei, Y. L., Zhang, Y., Sun, J., Xu, H. M., Ho, S. S. H., and Cao, J. J.: Light absorption properties and molecular profiles of HULIS in $PM_{2.5}$ emitted from biomass burning in traditional "Heated Kang" in Northwest China, Sci. Total Environ., 776, https://doi.org/10.1016/j.scitotenv.2021.146014, 2021.

Zhang, T., Shen, Z., Huang, S., Lei, Y., Zeng, Y., Sun, J., Zhang, Q., Ho, S. S. H., Xu, H., and Cao, J.: Optical properties, molecular characterizations, and oxidative potentials of different polarity levels of water-soluble organic matters in winter $PM_{2.5}$ in six China's megacities, Sci. Total Environ., 853, 158600, https://doi.org/10.1016/j.scitotenv.2022.158600, 2022a.

Zhang, T., Huang, S., Wang, D., Sun, J., Zhang, Q., Xu, H., Hang Ho, S. S., Cao, J., and Shen, Z.: Seasonal and diurnal variation of $PM_{2.5}$ HULIS over Xi'an in Northwest China: Optical properties, chemical functional group, and relationship with reactive oxygen species (ROS), Atmos. Environ., 268, 118782, https://doi.org/10.1016/j.atmosenv.2021.118782, 2022b.

Zhang, X. L., Lin, Y. H., Surratt, J. D., and Weber, R. J.: Sources, Composition and Absorption Angstrom Exponent of Light-absorbing Organic Components in

827 Aerosol Extracts from the Los Angeles Basin, Environ. Sci. Technol., 47,
828 3685-3693, http://doi.org/10.1021/es305047b, 2013.
829 Zhang, Y. L., Gao, G., Shi, K., Niu, C., Zhou, Y. Q., Qin, B. Q., and Liu, X. H.:
830 Absorption and fluorescence characteristics of rainwater CDOM and
831 contribution to Lake Taihu, China, Atmos. Environ., 98, 483-491,
832 http://doi.org/10.1016/j.atmosenv.2014.09.038, 2014.
833 Zhao, W. Y., Fu, P. Q., Yue, S. Y., Li, L. J., Xie, Q. R., Zhu, C., Wei, L. F., Ren, H.,
834 Li, P., Li, W. J., Sun, Y. L., Wang, Z. F., Kawamura, K., and Chen, J. M.:
835 Excitation-emission matrix fluorescence, molecular characterization and
836 compound-specific stable carbon isotopic composition of dissolved organic
837 matter in cloud water over Mt. Tai, Atmos. Environ., 213, 608-619,
838 http://doi.org/10.1016/j.atmosenv.2019.06.034, 2019.
839 Zheng, G., He, K., Duan, F., Cheng, Y., and Ma, Y.: Measurement of humic-like
840 substances in aerosols: a review, Environ. Pollut., 181, 301-314,
841 http://doi.org/10.1016/j.envpol.2013.05.055, 2013.
842 Zhou, Y., West, C. P., Hettiyadura, A. P. S., Niu, X., Wen, H., Cui, J., Shi, T., Pu, W.,
843 Wang, X., and Laskin, A.: Measurement report: Molecular composition, optical
844 properties, and radiative effects of water-soluble organic carbon in snowpack
845 samples from northern Xinjiang, China, Atmos. Chem. Phys., 21, 8531-8555,
846 https://doi.org/10.5194/acp-21-8531-2021, 2021.
847 Zhou, Y., Yao, X., Zhang, Y., Shi, K., Zhang, Y., Jeppesen, E., Gao, G., Zhu, G., and
848 Qin, B.: Potential rainfall-intensity and pH-driven shifts in the apparent

849 fluorescent composition of dissolved organic matter in rainwater, Environ.
850 Pollut., 224, 638-648, http://doi.org/10.1016/j.envpol.2017.02.048, 2017.

851

(a)

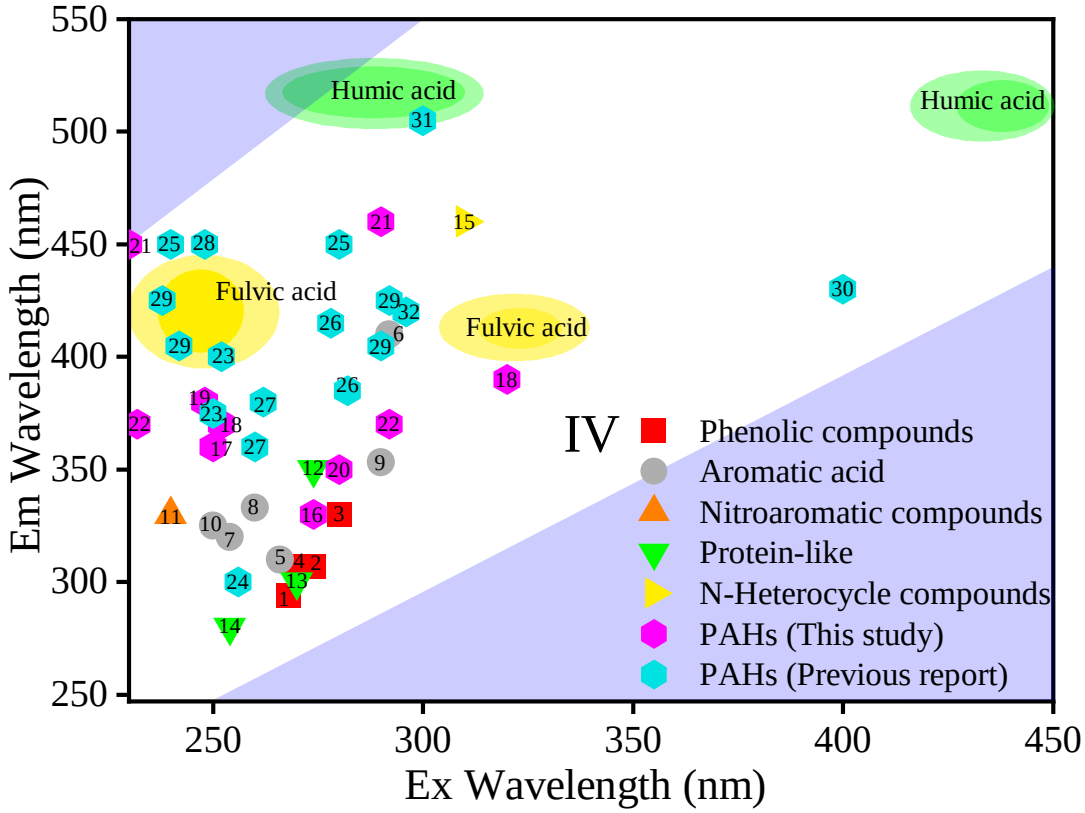

852

1: Phenol	2: Catechol	3: Hydroquinone
4: 2-Methoxyphenol	5: Benzoic acid	6: 2-Hydroxybenzoic acid
7: 4-Hydroxybenzoic acid	8: 4-Hydroxy-3, 5-dimethoxybenzoic acid	9: 3, 5-Dihydroxybenzoic acid
10: Vanillic acid	11: 4-Nitrocatechol	12: DL-Tryptophan
13: DL-Tryosine	14: Phenylalanine	15: midazole-2-formaldehyde
16: Naphthalene	17: Phenanthrene	18: Pyrene
19: Anthraquinone	20: 9-Fluorenone	21: 1-Naphthol
22:2-Napphthalenecarboxylic acid	23: Anthracene	24: Fluorene
25: Fluoranthene	26: Benzo-a-Anthracene	27: Chrysene
28: Benzo-b-Fluoranthene	29: Benzo-k-Fluoranthene	30: Perylene
31: Indeno-123cd-Pyrene	32: Benzo-ghi-Perylene	

853

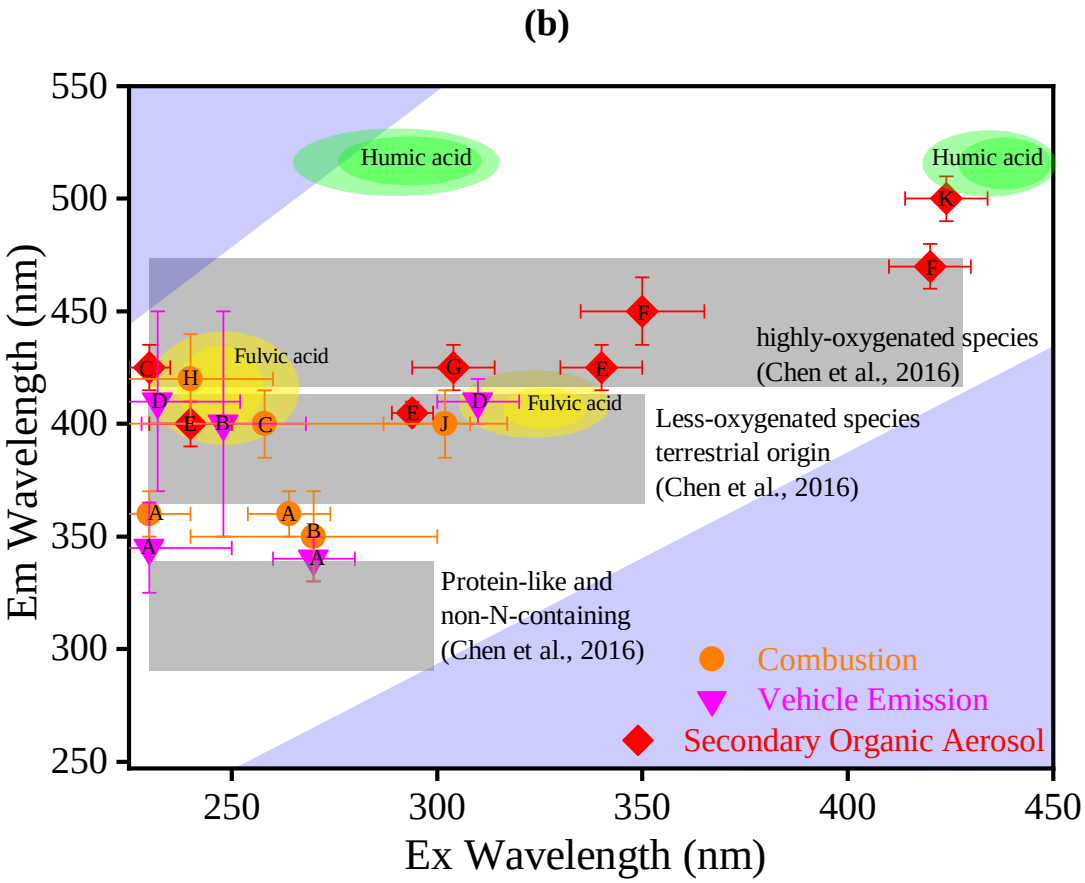

A: This study	B: Yang et al., 2022
C: Chen et al., 2020	D: Tang et al., 2020b
E: Hawkins et al., 2016	F: Bones et al., 2010
G: Lee et al., 2013	H: Mahamuni et al., 2020
J: Yan and Kim 2017	K: Powelson et al., 2014

Figure 1. Comparison of chemical characteristics of molecules assigned to each fluorescence component of BrC model compounds (a) and source WSOM (b).

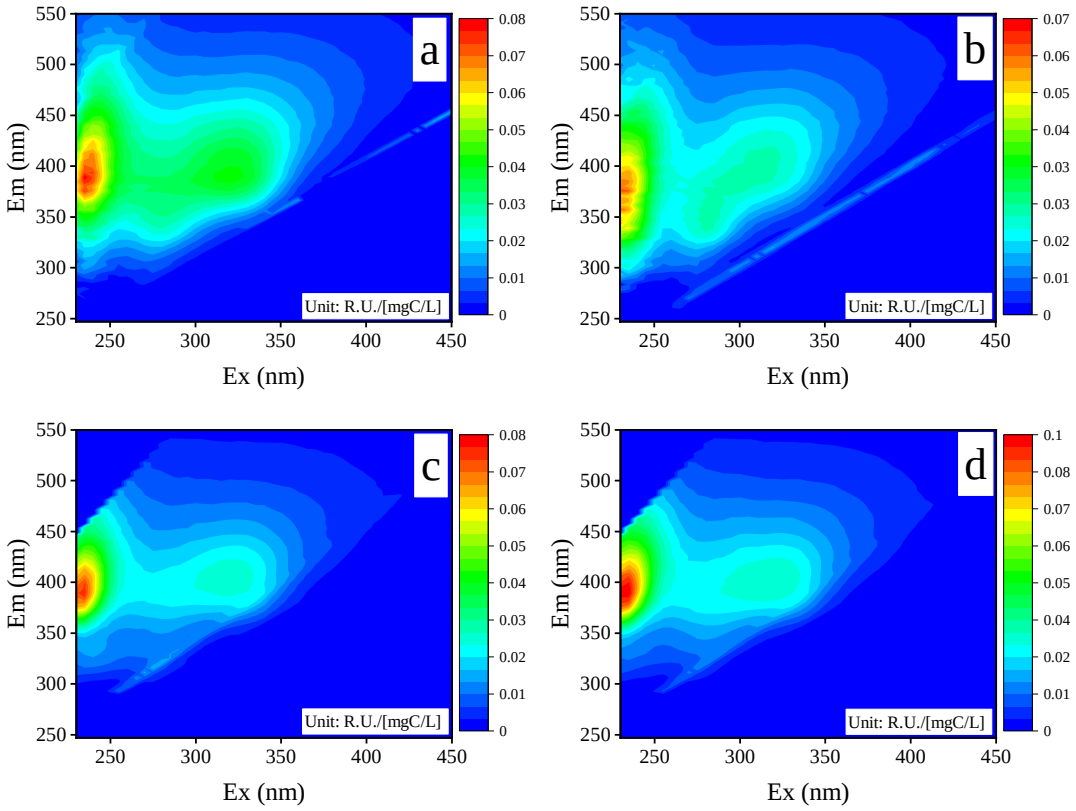

Figure 2. The 3D-EEM spectra of WSOM in atmospheric $PM_{2.5}$ samples (a: Chuzhou (CZ); b: Guangzhou (GZ); c: GZ wet season; d: GZ dry season)

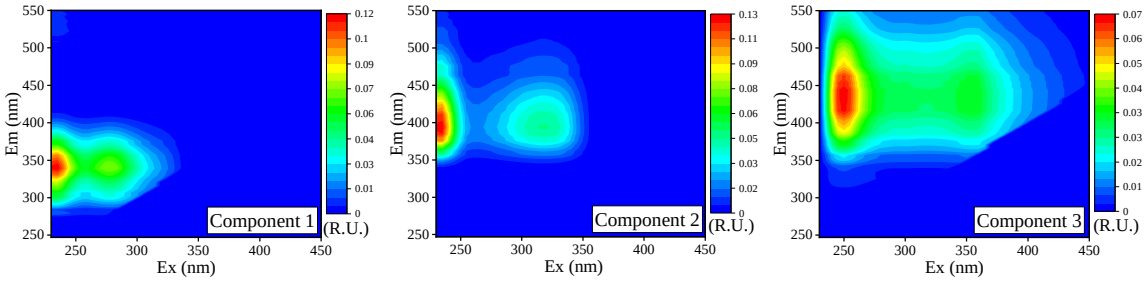

Figure 3. The EEM components derived from the PARAFAC model of WSOC in atmospheric $PM_{2.5}$ samples collected at Chuzhou (CZ) and Guangzhou (GZ) sites.

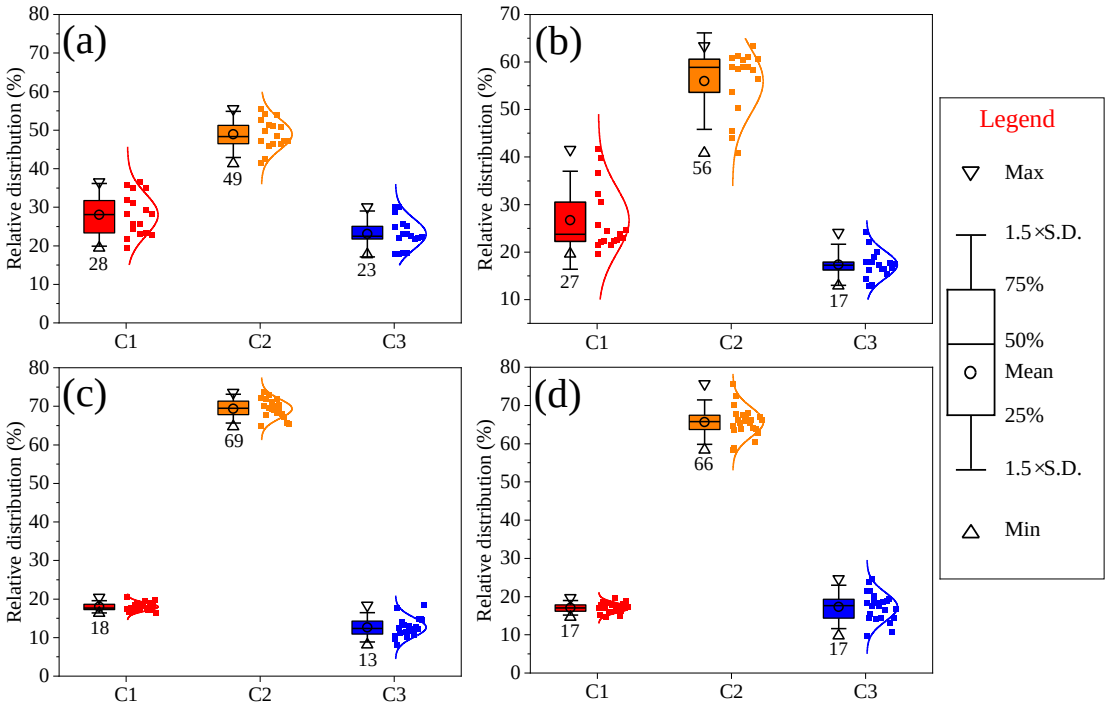

874

875 **Figure 4.** Relative contribution of individual fluorophores of atmospheric WSOM. (a:
876 Chuzhou (CZ); b: Guangzhou (GZ); c: wet season of GZ; d: dry season of GZ; the
877 colored box represents the data range of 25%-75%, the horizontal line within the box
878 represents the median line (50%), the error bar represents the 1.5 times the standard
879 deviation, the circle in the box represents the mean value of the data, the triangles in
880 the bottom and top represent the minimum and maximum values of the data; the dots
881 in the right of the box represent the overall data coupled with Gaussian distribution
882 line.)

883